INTERNATIONAL JOURNAL FOR NUMERICAL METHODS IN FLUIDS
Int. J. Numer. Meth. Fluids **31**: 513–522 (1999)

NATURAL CONVECTION HEAT TRANSFER IN THE ANNULAR REGION BETWEEN POROUS CONFOCAL ELLIPSES

E. SAATDJIAN[a], R. LAM[a] AND J.P.B. MOTA[b,*]

[a] *LEMTA-INPL, 2 Ave. de la Forêt de Haye, BP160, 54504 Vandoeuvre Cedex, France*
[b] *Dept. Química, Centro de Química Fina e Biotecnologia, FCT/UNL, 2825-114 Caparica, Portugal*

SUMMARY

The Darcy–Boussinesq equations are solved in two dimensions and in elliptical cylindrical co-ordinates using a second-order-accurate finite difference code and a very fine grid. For the limiting case of a circular geometry, the results show that a hysteresis loop is possible for some values of the radius ratio, in agreement both with previous calculations using cylindrical co-ordinates and with the available experimental data. For the general case of an annulus of elliptical cross-section, two configurations, blunt or slender, are considered. When the major axes are horizontal (blunt case) a hysteresis loop appears for a certain range of Raleigh numbers. For the slender configuration, when the major axes are vertical, a transition from a steady to a periodic regime (Hopf bifurcation) has been evidenced. In all cases, the heat transfer rate from the slender geometry is greater than that obtained in the blunt case. Copyright © 1999 John Wiley & Sons, Ltd.

KEY WORDS: natural convection; Darcy–Boussinesq equations; porous confocal ellipses

1. INTRODUCTION

Natural convection in the annular region between horizontal concentric cylinders, of elliptic or circular cross-section, and for fluid or porous layers is a problem that is not yet totally understood despite the numerous studies and the important industrial applications. The first experimental and numerical work concerning horizontal cylindrical porous layers was done by Caltagirone [1,2]. In the experiments, the porous medium consisted of glass beads and a colourless liquid both having the same index of refraction. The thermal field was visualized using the Christiansen effect. For a layer with a radius ratio $R = 2$, the experiments showed that the unicellular flow field remained stable for Rayleigh numbers not exceeding 65 ± 4. However, beyond this value of the Rayleigh number the experiments showed that the flow field became three-dimensional only on the top part of the layer. The flow field in the bottom part of the layer remained two-dimensional. Unfortunately, the numerical solution of the governing equations using a second-order finite difference technique did not confirm these results. The unicellular flow regime was found to be stable for Rayleigh numbers well beyond 65 ± 4. However, quantitative heat transfer data obtained experimentally was successfully compared with numerical results with a two-dimensional code.

* Correspondence to: Dept. Química, Centro de Química Fina e Biotecnologia, FCT/UNL, 2825-114 Caparica, Portugal.

CCC 0271–2091/99/180513–10$17.50

Received May 1998
Revised August 1998

A numerical study using the Galerkin method by Rao *et al.* [3] was able to reproduce the bifurcation point observed experimentally. For Rayleigh numbers beyond 65 ± 4, these authors obtain three different flow fields depending on the initial conditions. Himasekhar and Bau [4] use a regular perturbation expansion technique to study bifurcation phenomena for this problem. However, their analysis is valid for annuli of small radius ratio only.

The visualization experiments of Caltagirone have recently been redone by Charrier-Mojtabi *et al.* [5,6] on a very short cell. In this study, a unicellular flow regime was observed experimentally for Rayleigh numbers well beyond 65 ± 4. However, in some cases (the article is not very clear on this subject) a bicellular flow regime was observed when the Rayleigh number was decreased, and the flow field became unicellular once again for $Ra = 65 \pm 4$.

A new scenario of the bifurcation phenomena occurring in this layer has recently been presented by Mota and Saatdjian [7,8], whose results are based on the numerical solution of the two-dimensional equations. According to this study, for a layer of radius ratio $R = 2$ and for Rayleigh numbers above 65, a closed hysteresis loop is observed. On increasing the Rayleigh number, the unicellular flow field is stable until a value of about 110 is reached. At this point, the flow field becomes bicellular. If the Rayleigh number is decreased, the bicellular flow field is stable and the flow field becomes unicellular for a Rayleigh number of 65 ± 4. This scenario is consistent with the experiments and with most of the previously published theoretical and numerical data. However, the transitional Rayleigh number of 110 for which the unicellular flow regime becomes bicellular has not yet been confirmed.

Here, the Darcy–Oberbeck–Boussinesq equations are solved numerically in the porous annulus between horizontal cylinders of elliptic cross-section. Notice that the circular annulus and a flat plate are two limiting cases of the system considered here, the validity of the code can thus be checked. Concerning the general case, heat transfer is enhanced when the major axes are parallel to the vertical axis, a possible explanation is presented.

2. PROBLEM FORMULATION

Consider the annular porous region between two confocal elliptic horizontal cylinders. The inner and outer boundaries are kept at constant temperatures T_i and T_o respectively, with $T_i > T_o$. For this geometry, elliptical cylindrical co-ordinates are very practical and, furthermore, they are orthogonal. They are defined by the following transformations (blunt case):

$$x = a \cosh u \cos v, \qquad y = a \sinh u \sin v, \qquad z = z.$$

For this system of co-ordinates, the metric coefficients in the three directions are (h^*, h^*, 1) where

$$h^* = a\sqrt{\cosh^2 u - \cos^2 v},$$

and $2a$ is the focal distance. This geometry is completely specified by two dimensionless parameters: a_2/a_1 the ratio of the major axes of the outer and inner ellipses, and b_1/a_1 the ratio between the minor and the major axis of the inner ellipse. A sketch of the considered geometry is shown on Figure 1.

The governing dimensional system of equations to be solved is written below in vector form:

$$\nabla \cdot \mathbf{V} = 0,$$

$$\mathbf{V} = -\frac{k}{\mu}[\nabla P - \rho \mathbf{g}],$$

$$(\rho C_p)^* \frac{\partial T^*}{\partial t} + (\rho C_p)_f \mathbf{V}\cdot\nabla T^* = \lambda^* \nabla^2 T^*,$$

$$\rho = \rho_o[1 - \beta(T^* - T_o)].$$

These equations are the continuity equation for an incompressible fluid, Darcy's law for flow in a porous medium, the energy equation, and the fluid equation of state. The density variations with temperature are only considered in the buoyancy terms. Defining a dimensionless streamfunction ψ such that:

$$hU = \frac{\partial \psi}{\partial v}, \qquad hV = -\frac{\partial \psi}{\partial u},$$

where $h = h^*/a$ and taking the curl of the equation of motion, the following dimensionless system is obtained in two dimensions for the blunt configuration:

$$\frac{\partial T}{\partial t} + \frac{1}{h}\left[U\frac{\partial T}{\partial u} + V\frac{\partial T}{\partial v}\right] = \frac{1}{h^2}\left[\frac{\partial^2 T}{\partial u^2} + \frac{\partial^2 T}{\partial v^2}\right],$$

$$\frac{\partial^2 \psi}{\partial u^2} + \frac{\partial^2 \psi}{\partial v^2} = Ra^*\left[\sinh u \cos v \frac{\partial T}{\partial u} - \cosh u \sin v \frac{\partial T}{\partial v}\right].$$

The only dimensionless number appearing in these equations is the Rayleigh number, based on the focal radius a, defined by:

$$Ra = \frac{(\rho C_p)_f \beta g k a \Delta T}{\lambda^* \nu}.$$

Since the focal radius a depends on the geometry of the layer, the Rayleigh number used hereafter is based on the inner ellipse major axis, as in the cylindrical case. The dimensionless boundary conditions on the inner and outer walls are

$$T = 1, \ \psi = 0, \quad \text{for } u = u_1, \quad \text{inner wall},$$

$$T = 0, \ \psi = 0, \quad \text{for } u = u_2, \quad \text{outer wall}$$

and, furthermore, symmetry is assumed along the vertical axis.

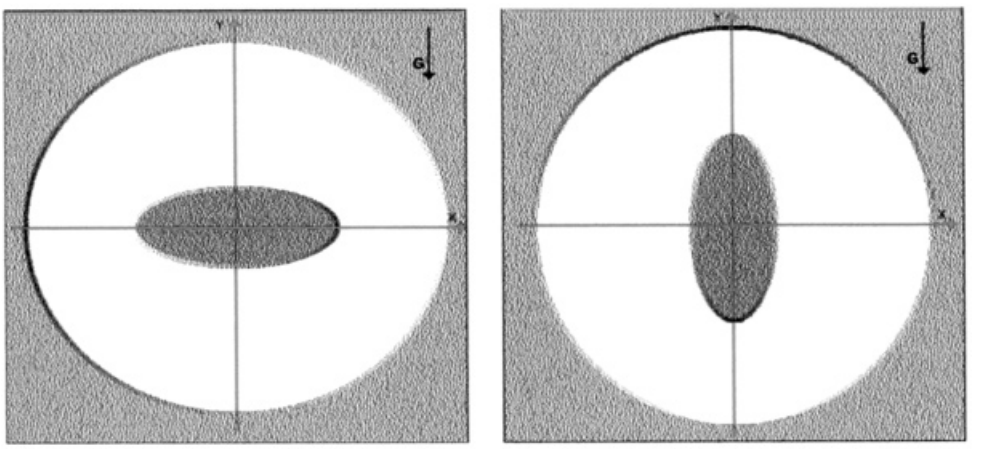

Figure 1. Annular region between confocal ellipses, blunt and slender configurations.

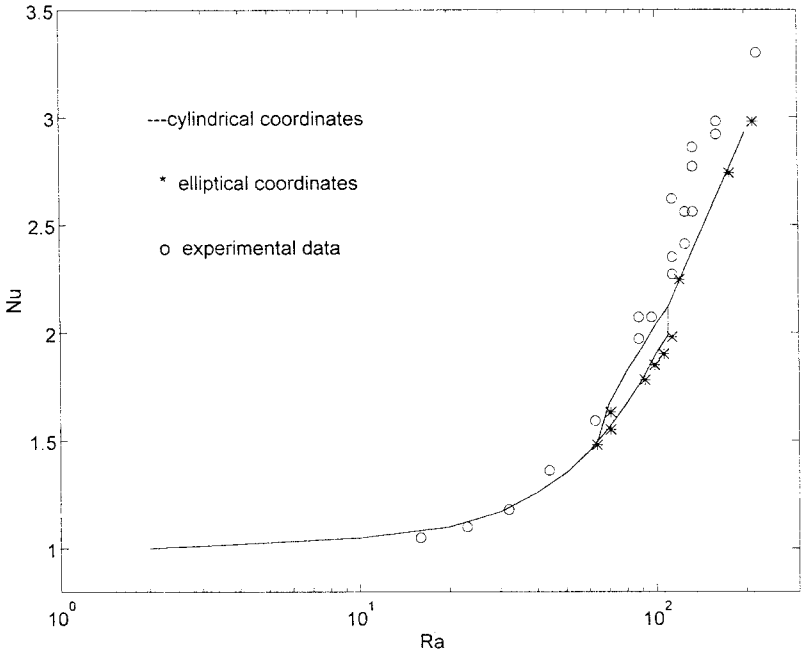

Figure 2. Nusselt number vs. Rayleigh number for $R = 2$; ○, experimental data; *, elliptical cylindrical co-ordiantes; —, cylindrical co-ordinates.

For the slender configuration (major axis parallel to gravity vector) the streamfunction equation to be solved in conjunction with the energy equation is

$$\frac{\partial^2 \psi}{\partial u^2} + \frac{\partial^2 \psi}{\partial v^2} = -Ra^* \left[\cosh u \sin v \frac{\partial T}{\partial u} + \sinh u \cos v \frac{\partial T}{\partial v} \right].$$

The average heat transfer loss from the inner wall can be estimated by integrating the local heat flux over the entire periphery. The average Nusselt number is defined as the ratio between the total heat loss and the heat loss for the case of pure conduction, or

$$Nu = \frac{Q_{\text{total}}}{Q_{\text{conduction}}} = \frac{u_1 - u_2}{2\pi} Q_{\text{total}},$$

where

$$Q_{\text{total}} = -\int_0^{2\pi} \frac{\partial T}{\partial u} \, \mathrm{d}v, \quad u = u_1 \text{ or } u = u_2.$$

3. NUMERICAL SOLUTION

The above partial differential equations are solved using finite differences on a 100×100 grid. The energy equation is solved using a second-order alternating direction scheme and the elliptic streamfunction equation is solved iteratively using a successive over relaxation technique. The code is very similar to the one used in [7,8] for the circular cylinder case. The calculations stop when the following test is successful for every grid point:

$$\left|\frac{T_{i,j}^{n+1} - T_{i,j}^{n}}{T_{i,j}^{n}}\right| < 10^{-5}.$$

For both cases, results were first obtained with a 51×81 grid covering half the porous layer. The grid size was then increased to 100×100. For practically all Rayleigh numbers considered

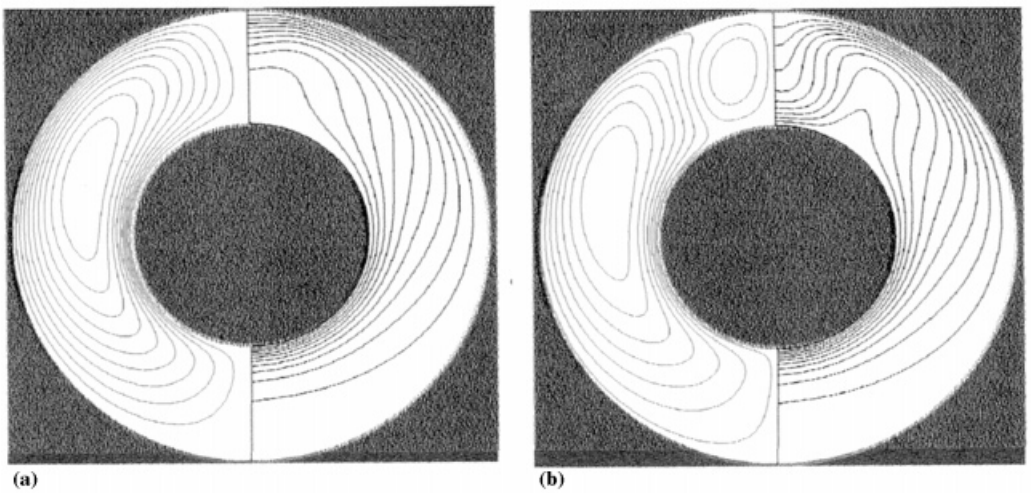

Figure 3. Isotherms and streamlines for $R = 2$ and $Ra = 100$. (a) Unicellular flow regime; (b) bicellular flow regime.

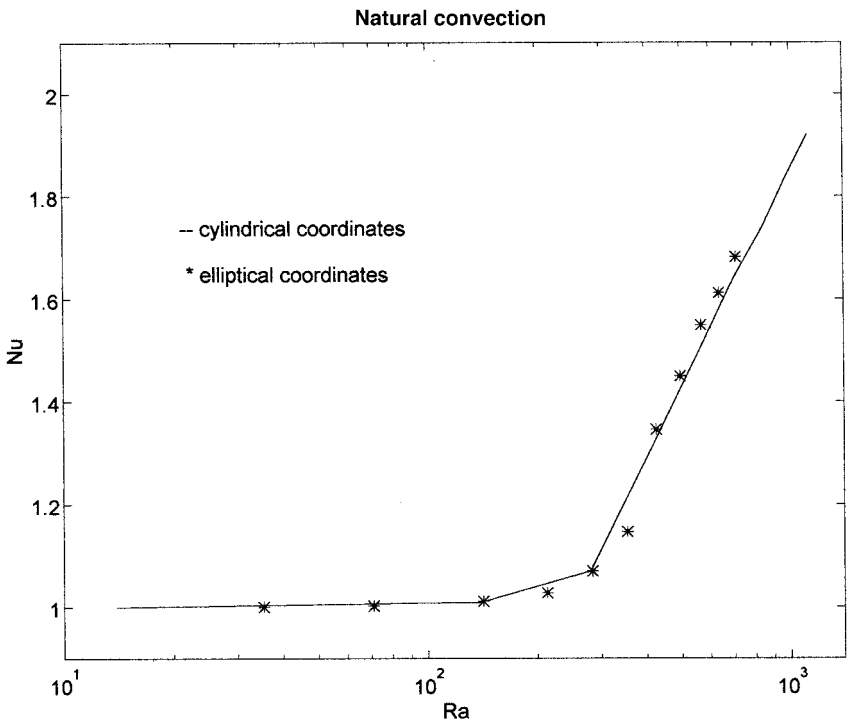

Figure 4. Nusselt number vs. Rayleigh number for $R = 1.2$; *, elliptical cylindrical co-ordinates; —, cylindrical co-ordinates.

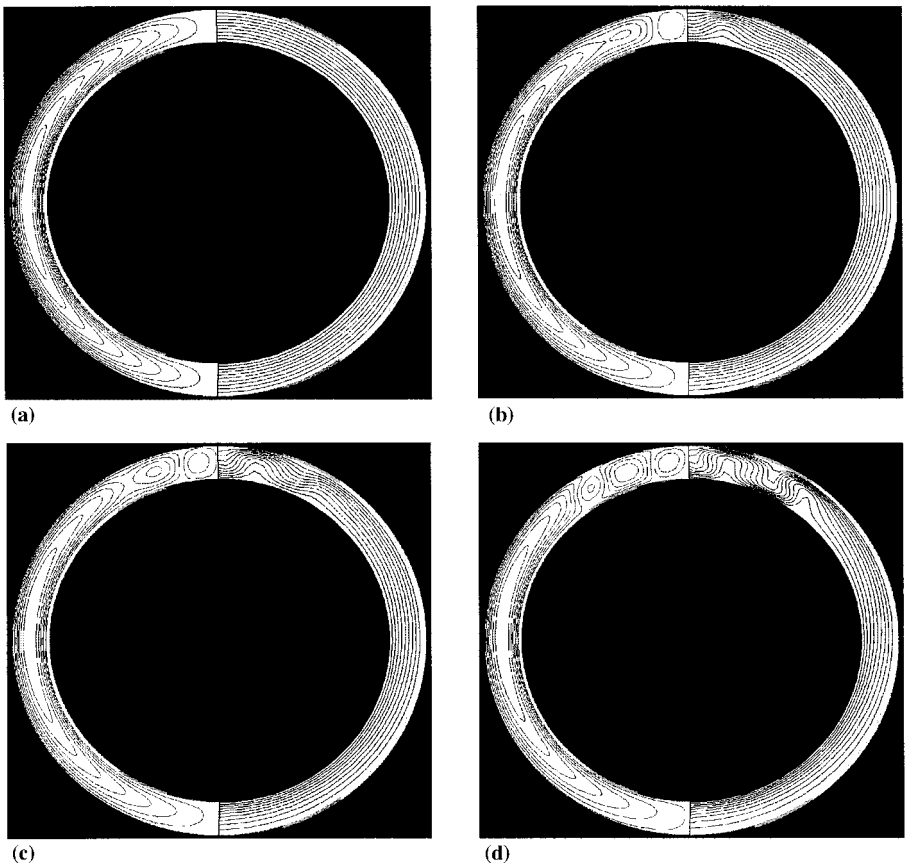

Figure 5. Isotherms and streamlines for $R = 1.2$. (a) Unicellular, (b) bicellular, (c) tricellular, (d) four cells.

here, the average Nusselt number calculated with the finer grid was less than 1% different to the value obtained with the coarser grid.

The local heat flux was evaluated using a fourth-order finite difference formula. In all calculations, the average Nusselt number evaluated at the outer wall differed by less than 1% from the value calculated at the inner wall.

In order to validate this code, data obtained for the limiting case of a circular porous layer is first compared with known, previously published results.

3.1. Concentric cylinder case

For a horizontal porous cylindrical annulus of radius ratio $R = 2$, Caltagirone [1,2] measured the average Nusselt number using a very long cell (end effects can be neglected). The code presented here was run with $a_2/a_1 = 2$ and $b_1/a_1 = 0.99$ in order to compare the present results with this data. Figure 2 shows a plot of the Nusselt number as a function of the Rayleigh number; the experimental data of Caltagirone [1,2], the numerical results of Mota and Saatdjian [7,8] using cylindrical co-ordinates and the results obtained with elliptical co-ordinates are all plotted on this figure. It can be seen that the present results compare very well with those obtained numerically using cylindrical co-ordinates. The agreement with the experimental data is excellent for Rayleigh numbers up to 100 and very good for Rayleigh

numbers above 100. Notice that, on increasing the Rayleigh number, the numerical solution predicts that the unicellular flow regime (Figure 3(a)) becomes bicellular (Figure 3(b)) for a Rayleigh number of 110. However, as the Rayleigh number is decreased, the bicellular

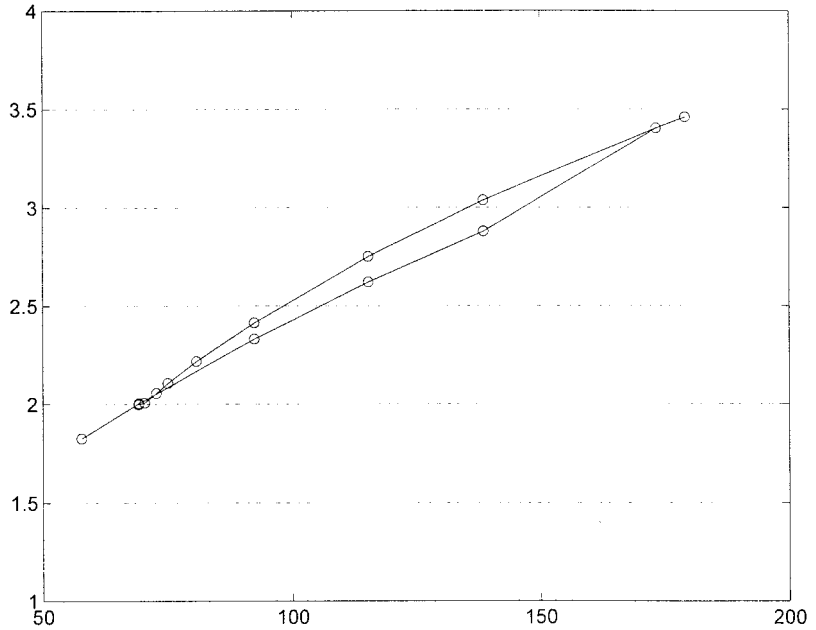

Figure 6. Nusselt number vs. Rayleigh number for $a_2/a_1 = 2$, $b_1/a_1 = 0.5$, blunt configuration.

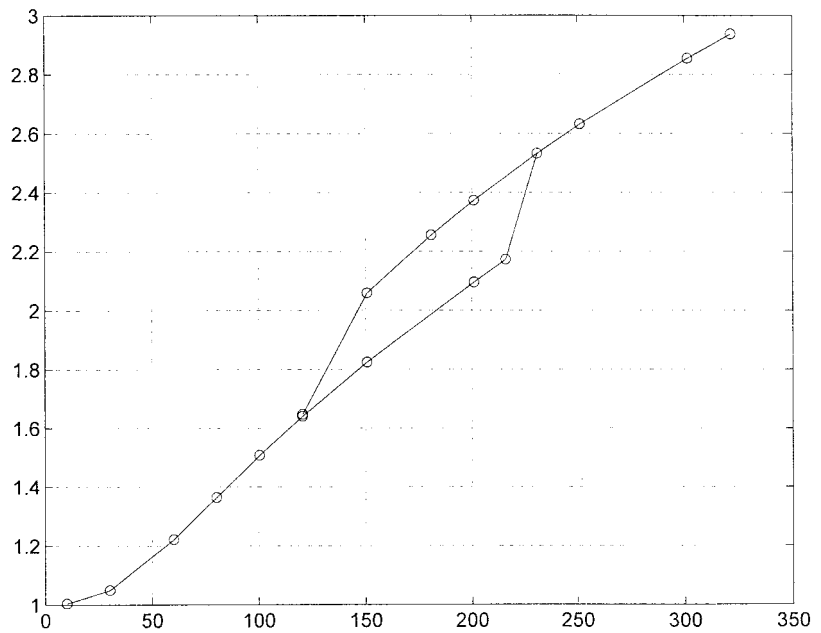

Figure 7. Nusselt number vs. Rayleigh number for $a_2/a_1 = 1.1$, $b_1/a_1 = 0.1$, blunt configuration.

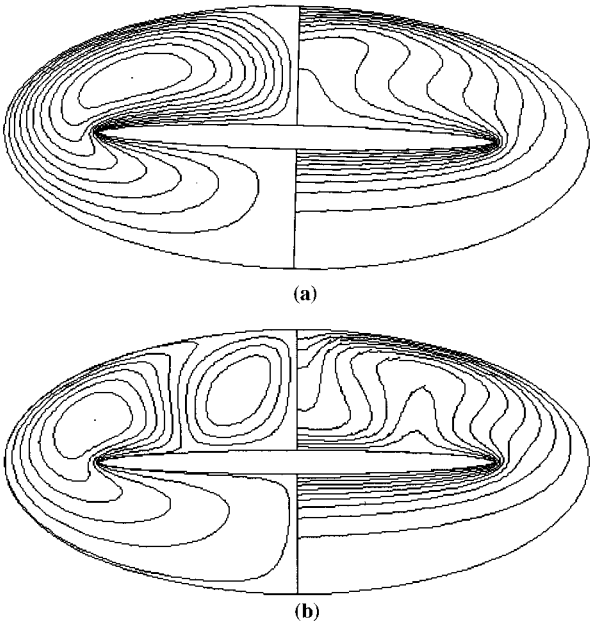

Figure 8. Isotherms and streamlines for $a_2/a_1 = 1.1$, $b_1/a_1 = 0.1$. (a) Unicellular, (b) bicellular flow regime; $Ra = 200$.

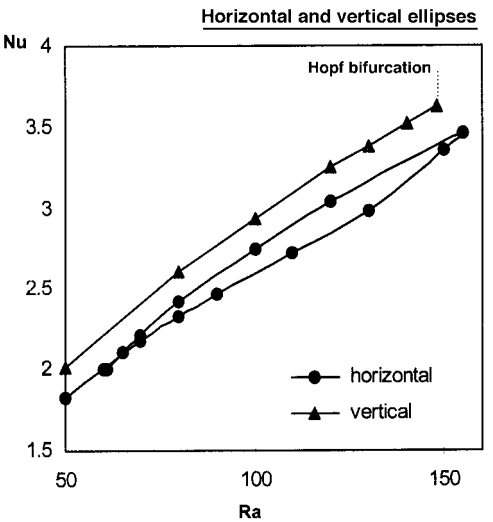

Figure 9. Nusselt number vs. Rayleigh number for $a_2/a_1 = 2$, $b_1/a_1 = 0.5$, a comparison between blunt and slender configurations.

becomes unicellular for a Rayleigh number of 65; these values are the same as those obtained with the code in cylindrical co-ordinates. The bifurcation value of the Rayleigh number (65 ± 4) is in good agreement with the experimental data.

The bicellular flow regime has recently been observed on a cell of very small aspect ratio by Charrier Mojtabi [5]. At the time, it was believed that three possible flow regimes were possible for certain Rayleigh numbers (see [3]). It has now been established [9] that the multicellular regime obtained numerically converges into the unicellular regime if a more severe convergence test is imposed.

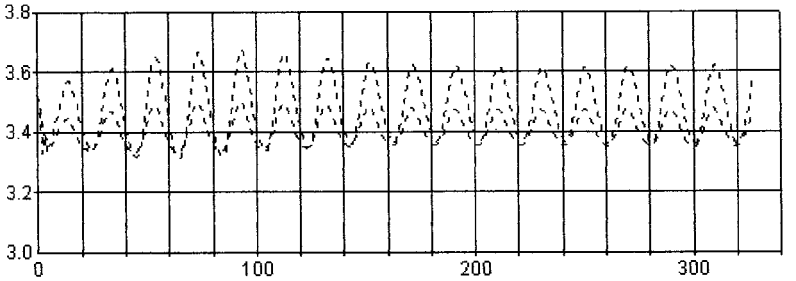

Figure 10. Nusselt number vs. time for $a_2/a_1 = 2$, $b_1/a_1 = 0.5$, slender configuration; $Ra = 150$.

For a radius ratio of $R = 1.2$, Figure 4 gives a plot of the Nusselt number versus the Rayleigh number, numerical results obtained with both cylindrical and elliptical co-ordinates are shown. For this case, the number of cells in half the layer varies from one to four, as shown in Figure 5. These last results, for a layer of small radius ratio, are in agreement with the bifurcation analysis of Himasekhar and Bau [4].

3.2. Elliptic porous layer

Results obtained for the case where the major axis is horizontal (blunt configuration) are first presented. For a geometry defined by $a_2/a_1 = 2$ and $b_1/a_1 = 0.5$, a plot of the Nusselt number versus the Rayleigh number is shown in Figure 6. As in the concentric case of the same radius ratio, a hysteresis loop is obtained between Rayleigh numbers 69 and 173. The heat transfer rate from an annulus of elliptic cross-section is greater than that obtained from the circular annulus of the same radius ratio.

For an annulus defined by $a_2/a_1 = 1.1$ and $b_1/a_1 = 0.1$, the plot of the Nusselt number versus the Rayleigh number is shown in Figure 7. Notice that despite the small major axis ratio, and unlike the cylindrical case, a hysteresis loop is again obtained. Figure 8 shows the isotherms and the streamlines for the two possible regimes at a Rayleigh number of 200. For this value of the eccentricity ($\epsilon = 0.1$), the geometry is similar to a horizontal flat plate and the secondary cell is well-defined and stable.

Calculations for the slender configuration (Figure 1(b)) have also been performed. For the unicellular regime, the velocities are greater than those obtained in the blunt configuration. So, in all cases, the overall heat transfer from the walls to the fluid is greater in this configuration. This phenomenon has also been noted for fluid layers [10,11], and is attributed to curvature. For Rayleigh numbers between 50 and 150, Figure 9 shows the average Nusselt number for both configurations, the radius ratio and the eccentricity are 2 and 0.5 respectively. Notice that the curve for the slender configuration is always on top of the one for the blunt configuration.

An interesting phenomenon occurs for the slender configuration once a high enough Rayleigh number is reached. Instead of creating a secondary cell, a Hopf bifurcation is encountered. In Figure 10, the average Nusselt number on both walls is plotted versus time. As can be seen, the average Nusselt number varies periodically with time. A stability analysis should be able to confirm this observation.

4. CONCLUSIONS

The Darcy–Boussinesq natural convection equations are solved using finite differences on a confocal elliptical porous layer; the circular annulus and a horizontal flat plate are two limiting

cases of this geometry. An implicit alternating direction scheme is used to solve the energy equation and an iterative scheme is implemented for the streamfunction equation. The results obtained for the circular annulus confirm those obtained previously using cylindrical co-ordinates. For the elliptical case, the heat transfer from a layer with vertical major axes is greater than that from a layer with horizontal major axes. When the major axes are vertical, a Hopf bifurcation (instead of the formation of a secondary cell) is observed for Rayleigh numbers above a certain limit.

REFERENCES

1. J.P. Caltagirone, 'Thermoconvective instabilities in porous medium bounded by two concentric horizontal cylinders', *J. Fluid Mech*., **76**, 337–362 (1976).
2. J.P. Caltagirone, 'Instabilités thermoconvectives en milieu poreux', *Thèse de Doctorat d'Etat*, Université Pierre et Marie Curie (Paris VI), 1976.
3. Y.F. Rao *et al*., 'Steady and transient analyses of natural convection in a horizontal porous annulus using the Galerkin method', *ASME J. Heat Transf*., **109**, 919–927 (1987).
4. K. Himasekhar and H.H. Bau, 'Two-dimensional bifurcation phenomena in thermal convection in horizontal concentric annuli containing saturated porous media', *J. Fluid Mech*., **187**, 267–300 (1988).
5. M.C. Charrier Mojtabi, 'Etude numerique, theorique et experimentale des écoulements thermoconvectifs bidimensionnels et tridimensionnels en couche amlulaire poreuse horizontale', *Thèse de Doctorat d'Etat*, Université de Bordeaux I, 1993.
6. M.C. Charrier Mojtabi *et al*., 'Numerical and experimental study of multicellular free convection flows in an annular porous layer', *Int. J. Heat Mass Transf*., **12**, 3061–3074 (1991).
7. J.P.B. Mota and E. Saatdjian, 'Natural convection in a porous, horizontal cylindrical annulus', *ASME J. Heat Transf*., **116**, 621–626 (1994).
8. J.P.B. Mota and E. Santdjian, 'Natural convection in porous cylindrical annuli', *Int. J. Numer. Methods Heat Fluid Flow*, **5**, 3–12 (1995).
9. M.C. Charrier Mojtabi, Private communication.
10. J.H. Lee and T.S. Lee, 'Natural convection in the annuli between horizontal confocal elliptic cylinders', *Int. J. Heat Mass Transf*., **24**, 1739–1742 (1981).
11. G.D. Raithby and K.G.T. Hollands, 'Laminar and turbulent free convection from elliptic cylinders, with a vertical plate and horizontal circular cylinder as special cases', *ASME J. Heat Transf*., **98**, 72–80 (1976).

